NREL/TP-257-4517 • UC Category: 261 • DE92001187

The NREL Teetering Hub Rotor Code: Final Results and Conclusions

A.D. Wright
C.P. Butterfield

National Renewable Energy Laboratory
(formerly the Solar Energy Research Institute)
1617 Cole Boulevard
Golden, Colorado 80401-3393
A Division of Midwest Research Institute
Operated for the U.S. Department of Energy
under Contract No. DE-AC02-83CH10093

December 1991

On September 16, 1991, the Solar Energy Research Institute was designated a national laboratory, and its name was changed to the National Renewable Energy Laboratory.

NOTICE

Printed in the United States of America
Available from:
National Technical Information Service
U.S. Department of Commerce
5285 Port Royal Road
Springfield, VA 22161

Price: Microfiche A01
Printed Copy A03

Codes are used for pricing all publications. The code is determined by the number of pages in the publication. Information pertaining to the pricing codes can be found in the current issue of the following publications which are generally available in most libraries: *Energy Research Abstracts (ERA)*; *Government Reports Announcements* and Index (*GRA* and I); *Scientific and Technical Abstract Reports (STAR)*; and publication NTIS-PR-360 available from NTIS at the above address.

The NREL Teetering Hub Rotor Code: Final Results and Conclusions

A. D. Wright
C. P. Butterfield

National Renewable Energy Lab
(formerly the Solar Energy Research Institute)
1617 Cole Boulevard
Golden, CO 80401

Abstract

Accurately predicting wind turbine blade loads and response is important for the proper design of wind turbines. The need to accurately predict both deterministic and stochastic blade loads is now widely recognized.

Previous rotor code development and validation efforts at NREL have concentrated on prediction of deterministic and stochastic blade loads for rigid hub rotors. During the past year this effort was expanded for predicting blade and shaft loads for two-bladed teetering hub rotors. The NREL (formerly SERI) Teetering Rotor Analysis Program (STRAP), a derivative of the Force and Loads Analysis Program (FLAP), can include the effects of rotor undersling, delta-3 and the effects of a concentrated hub mass. The degrees of freedom include rotor teeter and symmetric and asymmetric rotor flap modes. A time-dependent, prescribed yaw motion can also be input to the code. Loads due to turbulent wind inputs are also calculated.

In this paper, final code modifications, final comparisons of load predictions to test data, and finally, the direction for new code development activities at NREL will be described.

Nomenclature

C_L	Lift coefficient
CODEC	Coherence in the VEERS model (see reference
D	Dimensional
R	Rotor radius
Z_o	Terrain surface roughness
PSD	Power spectral density
U_*	Wind shear velocity (see reference 5)
β	Parameter in VEERS model (see reference 5)
P	Per rotor revolution
m/s	Meters per second
m	Meters
d	Distance of a concentrated hub mass from point of blade apex (see Figure 1)
u	Undersling: distance of teeter axis downwind of blade's apex (see Figure 1)
M_{hub}	Concentrated hub mass
S_i	Generalized coordinate for the i'th mode
δ_3	Delta-3 hinge angle (deg.)

Introduction

The ability to predict turbine loads and responses for a variety of wind turbines undergoing various operating conditions is a major goal of the federal Wind Energy Program. Previous structural dynamic modeling efforts at NREL have concentrated on three-bladed rigid hub rotors (1), (2), (3). During the past year, a two-bladed teetering hub rotor code has been in a stage of final refinement and validation.

This code models the teetering and flap-bending blade motion of a teetering hub rotor. The model includes such effects as undersling, hub mass, delta-3, turbulent wind inputs and a prescribed yaw motion. Also included is the ability to model teeter stops via springs and dampers.

The need to include turbulent wind inputs in structural dynamic models for wind turbines is now widely accepted. Wind turbine blade responses to turbulent winds have been described in (1), (2), (3), and (4).

In this paper the Three-Dimensional Wind Simulation Model (5) developed by P. S. Veers will be used to provide turbulent windspeed fluctuations for STRAP. It will be referred to as the VEERS model. Rotor teeter and load predictions from STRAP will be compared to test data for two different data cases, for a particular two-bladed field turbine, now operating in a California windfarm.

Both deterministic and stochastic load and response cases will be shown. Conclusions and recommendations for future code development will be made.

Code Highlights

The NREL (formerly SERI) Teetering Rotor Analysis Program (STRAP) is basically a derivative of FLAP (Force and Loads Analysis Program) (6). Equations of motion for blade flap motion were reformulated to correctly include the effects of rotor teeter motion; including the effects of delta-3, undersling, and hub mass.

Figure 1 shows the two-bladed teetering hub wind turbine which is modeled by this analysis. The rotor has a teetering hinge at point A which may be located a distance (u-ft) downwind of the hub. It may also include the effects of delta-3 (although the δ_3 angle was zero for the turbine to be described). The total rotor mass includes the distributed mass of the blades plus the mass of the hub. The hubmass is modeled as a concentrated mass (Mhub) located at a distance downwind of the hub center. This point locates the hub center of gravity location. The total rotor center of gravity location may be at a different point, due to the effects of the blade's mass and precone.

The model includes degrees of freedom of rotor teeter and three rotor elastic flap modes: two symmetric modes and one asymmetric mode, shown in Figure 2. The rotor rotation speed is assumed to be constant. Although turbine yaw is not considered to be a degree of freedom, a time-dependent prescribed yaw motion can be input to the code.

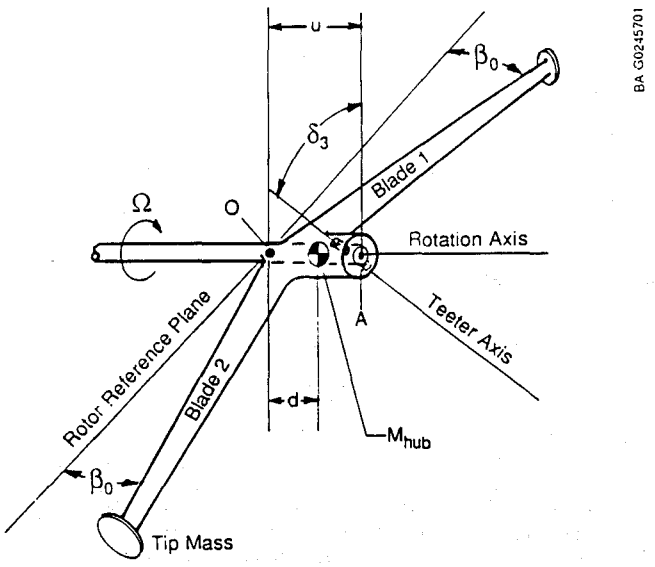

Figure 1. Rotor Geometry

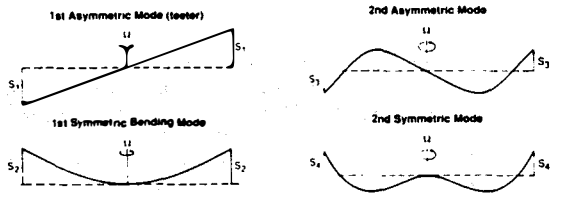

Figure 2. STRAP Modeshapes

The code can be used to obtain steady state responses to deterministic inputs, such as gravity, wind shear, tower shadow, and constant yaw rate. The code can also be run in a "time-marching" solution process, with inputs of time series turbulent windspeeds made from a separate file, such as that generated by the VEERS turbulence model (5). Stochastic blade loads, teeter response, and turbine low-speed shaft loads are then calculated.

The aerodynamic model used in the version of STRAP reported here is a simple quasi-steady aerodynamics model based on blade element-momentum theory (6). In this paper, nonlinear equations are used to accurately model steady 2-D lift and drag profiles for the LS(1) airfoil. For high angles of attack, the poststall synthesization routine is used (7). These methods represent a deviation in the method of lift and drag coefficient calculation of previous FLAP comparisons in which lift coefficient is a linear function of angle of attack.

Presently, a more sophisticated aerodynamics model is being added to STRAP based on Weber (8). This model will include table look-up subroutines for determination of lift and drag coefficients for various airfoils of different thicknesses at various Reynold's numbers. Iteration is performed in order to determine axial induction factors.

STRAP response and loads predictions are compared to test data taken from a two-bladed teetering hub turbine described in the next section. Two 10-minute data cases are analyzed to determine windspeed inputs, teeter test response, and blade flap bending moments at the root and 60% blade stations. The turbine and data set-up descriptions follow.

Turbine and Test Description

A 24-m (80 ft) diameter turbine, designed by ESI Inc. was selected as the test machine. It was chosen because a substantial data base existed, and it appeared to be a popular configuration for advanced turbine development. The ESI-80 wind turbine is a two-bladed, fixed pitch, free yaw, downwind system featuring wood epoxy composite rotor blades. These blades use LS(1)-04XX airfoils with thickness distribution and planform shown in Figure 3. This blade has a chord taper ratio of 2.2 beginning at the 30% blade radial station. Figure 3 also describes the linear trailing-edge-drop twist distribution of 4.0°. Blade stiffness and mass distributions are shown in Figures 4 and 5. The blade pitch is set to zero degrees measured at the 75% blade span. The rotor has a solidity of 0.035 and a coning angle of 7 degrees, angled away from the tower. The teetered rotor has a delta-three angle of zero degrees and rotates at a constant rotational speed of 60 rpm. Aerodynamically shaped tip vanes mounted at the blade tip, perpendicular to the spanwise axis, provide overspeed protection and assist in high wind stops. The turbine has a 30:1 gear ratio, planetary gearbox, which is coupled to a three-phase, 480 Volt, 300 kW induction generator. Table 1 summarizes the major turbine specifications for the test turbine.

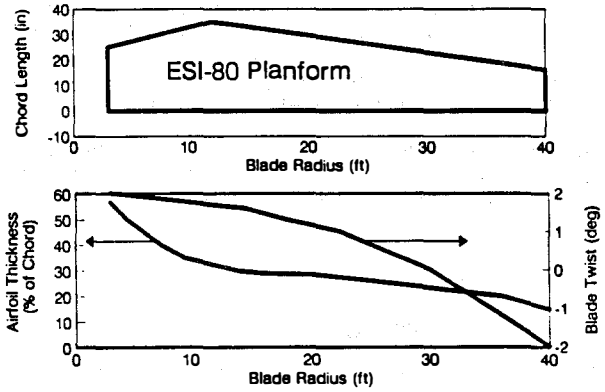

Figure 3. ESI-80 Blade Planform, Thickness, and Twist

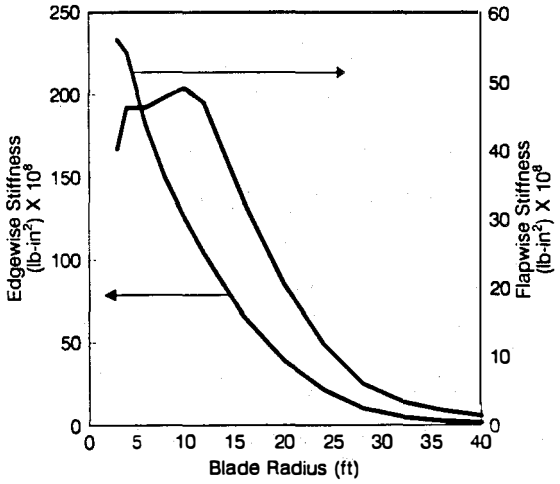

Figure 4. ESI-80 Blade Stiffness Distribution

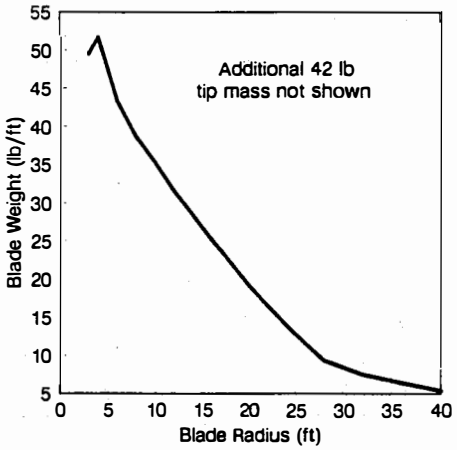

Figure 5. ESI-80 Blade Weight Distribution

Table 1

ESI-80 TURBINE SPECIFICATIONS

Rated Power	250 kW
Rated Wind Speed	20.3 m/s (45 mph)
Rotor	
Diameter	24.5 m (80 feet)
Rotor Type	Teetered - Stall Control
Rotor Orientation	Downwind
Blade Construction	Wood-Epoxy
Composite	
Rotor Airfoil	NASA LS(1) 0417
Tip Speed	77.9 m/s (173 mph)
Cut-in Windspeed	5.9 m/s (13 mph)
Rotor rpm	60 rpm
Generator Type	300 kW, Induction,
Three Phase	
Gearbox	Planetary
Hub Height	24.9 m (81.5 feet)
Tower	Open - Truss
Pitch Control	None
Yaw	Passive
Overspeed Control	Tip Vanes
Total System Weight	9750 kg (21,500 lb)
Coning	7°

Rotating Natural Frequencies

Teeter	1 Hz
First Symmetrical Flapwise	2 Hz
Second Symmetrical Flapwise	7.8 Hz
First Edgewise	5.9 Hz
Second Antisymmetrical Flapwise	12 Hz

Instrumentation Description

The ESI-80 test turbine was located in Altamont Pass near Tracy, California. A 37-m (120 ft) meteorological (MET) tower was located 50-m (160 ft) to the west of the wind turbine in the prevailing wind direction, as seen in Figure 6.

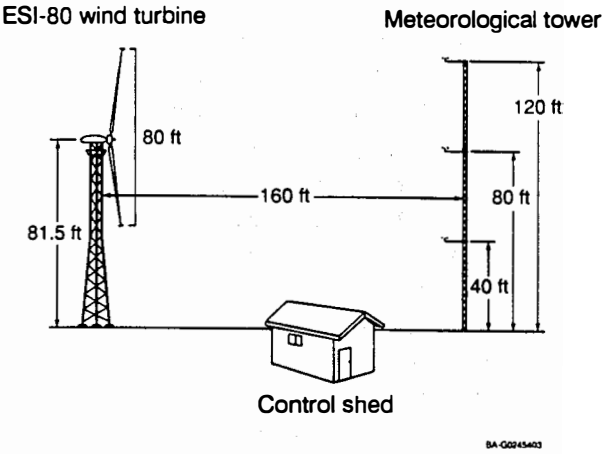

Figure 6. Test Site Layout

Table 2 lists the test channels that were measured during the test program, which was carried out with support of the Electric Power Research Institute (EPRI) in 1985. The locations of these transducers are indicated in Figure 7. All of the transducers represented in this figure were full bridge strain gage circuits except for items 10 and 12, the rotor azimuth position sensor and the yaw position sensor, respectively. Both of these instruments were built by ESI. Both converted rotary motion to linear motion using circular cams and linear potentiometers, which were energized by a simple power supply circuit. A 0-10 ma current loop analog signal, from each transducer-signal conditioner pair on the turbine, was fed through a 19-twisted-pair, shielded instrumentation cable down to the control shed.

Four Gill Propeller Vane anemometers and an R.M. Young signal conditioner and calibrator were used to condition windspeed and direction signal. These anemometers were located at 12.2-m (40 ft), 24.5-m (80 t), 36.7-m (120ft) altitudes on the MET tower.

Data signals for all of the transducers were terminated inside the control shed, where the signals were recorded on a Vetter Model-G, 16 channel, analog tape recorder. Not all 21 channels could be recorded simultaneously. Sixteen out of 21 channels were selected based on the goals of each test. The turbine is shown in Figure 7.

Test Data Cases

Two 10-minute data cases of different mean windspeed were compared to STRAP code predictions. Statistical values representative over the rotor disk were calculated by computing statistics for each anemometer and then averaging these results. This average was obtained for each data set. A power law shear coefficient was also determined for each case.

Table 3 shows summaries of the windspeed statistics for the two data cases, as well as turbine yaw error and the power law shear coefficient.

Table 2

MEASURED PARAMETERS
FOR THE
ESI-80 TEST TURBINE

Item	Description
1	Windspeed @ 31.5 m (120 ft)
2	Wind Direction @ 31.5 m (120 ft)
3	Windspeed @ 24.5 m (80 ft)
4	Wind Direction @ 24.5 m (80 ft)
5	Windspeed @ 12.2 m (40 ft)
6	Wind Direction @ 12.2 (40 ft)
7	Primary Tower Leg Load
8	North Hinged Tower Leg Load
9	South Hinged Tower Leg Load
10	Rotor Azimuth Position
11	Teeter Angle
12	Yaw Angle
13	Blade Root Flap Bending
14	Blade Flap Bending @ 60% R
15	Low-Speed Shaft Torque
16	Blade Root Edgewise Bending
17	Electrical Power
18	Electrical Current
19	20 Apparent Power (kVA)
20	Apparent Power (kVA)
21	Low-Speed Shaft Thrust

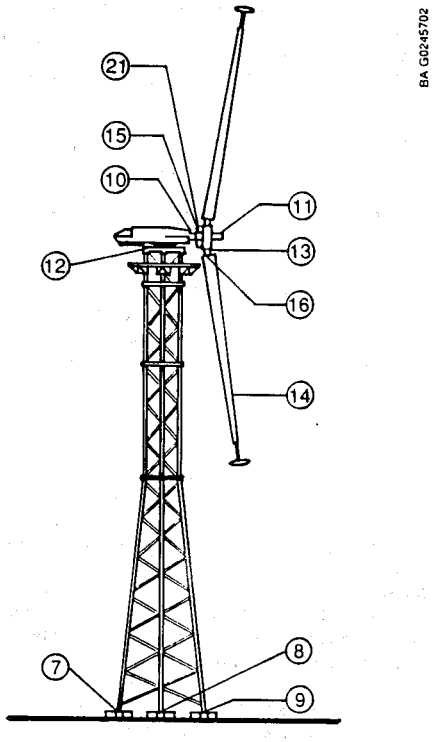

Figure 7. Turbine Instrumentation

Table 3. Statistics for the Two Data Cases

	Data Case 1	Data Case 2
Mean Windspeed (ft/s)	53.0	33.1
Standard Deviation (ft/s)	6.4	2.6
Power Law Shear Coefficient	.193	.164
Yaw Error (deg.)	4	13

The loads and teeter data are binned according to rotor azimuth position. The resulting "azimuth averaged" signals are then extracted from the data and fit with discrete Fourier series in order to determine the harmonic content up to a frequency of eight times the rotor rotation rate (8-P).

In addition, power spectral densities (PSDs) of each signal are calculated for comparison to stochastic loads and teeter predictions. The azimuth averaged responses are not removed before power spectral densities are computed, as later seen. The test data PSDs contain the sum of the deterministic and stochastic components. It is felt that the code should calculate the total response due to turbulence, shear, and tower shadow, and comparisons should be made for the total rotor response. The purpose for separating the azimuth averaged response is for harmonic comparisons to the steady state (deterministic) cases.

Turbulence Simulation Method

For turbulent wind simulation, the Sandia Three-Dimensional Wind Simulation (5), developed by VEERS, is used. This code is used to simulate the longitudinal component of turbulence (perpendicular to the rotor disk in nonyawed flow). A full three-component field of turbulence is not calculated; only the longitudinal component was calculated.

The simulation method is used to obtain "rotationally sampled" windspeed, although nonrotating windspeed can also be obtained from the model with minor modifications. The basic approach of this method is to simulate windspeed time series at several points in a plane perpendicular to the mean wind direction and to propagate the time series in the mean wind direction at the mean windspeed. These signals are then rotationally sampled in the code.

Various spectral models can be chosen in this code for calculation of the fixed point Power Spectral Density (PSD). For the cases shown here the Solari model was used (5). The coherence model used in (5) is the exponential type with some modification due to Solari.

Parameters are needed such as number of blades, number of points per revolution, number of and location of points along the blade span. Also, terrain surface roughness, shear, and coherence decrement are needed.

For the simulation performed for this turbine, 24 points per revolution were used. Turbulence was simulated at three blade radial locations: the hub, 0.5 R, and 1.0 R radial stations. The high number of azimuth points was chosen by information provided by Winkelaar in (12).

The Solari model calculated the single point power spectral densities. Inputs to this model include U_* (shear velocity) and β (5). These parameters are normally calculated within the VEERS model upon input of such parameters as surface roughness (Z_o) and turbulence intensity (standard deviation of windspeed divided by mean windspeed). However, for these cases, a least-squares curve fitting method was used to fit the Solari model equation to the hubheight

anemometer data PSD. The "best fit" parameter values for U_* and β were then determined for each data set in the frequency range of .01 to 1 Hz. Input values for Z_o, shear, etc. were then adjusted to give hubheight wind PSDs which closely represented that obtained from the actual hubheight test data. As a check on the accuracy of VEERS model generated windspeeds, a PSD of hubheight windspeed, generated by the VEERS model was compared to the PSD of hubheight anemometer test data, shown in Figures 8 to 9 for the two data sets. Evident in these figures is the rapid dropoff in the anemometer test data PSD above 1 Hz. The coherence decrement was set arbitrarily. The effects of this parameter on predicted results will be shown. Exact values for this parameter could not be obtained from anemometer data.

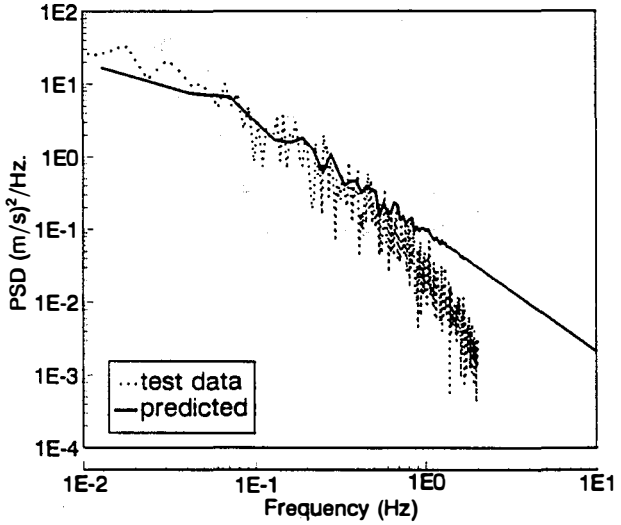

Figure 8. Spectra of Hub Height Anemometer (Case 1)

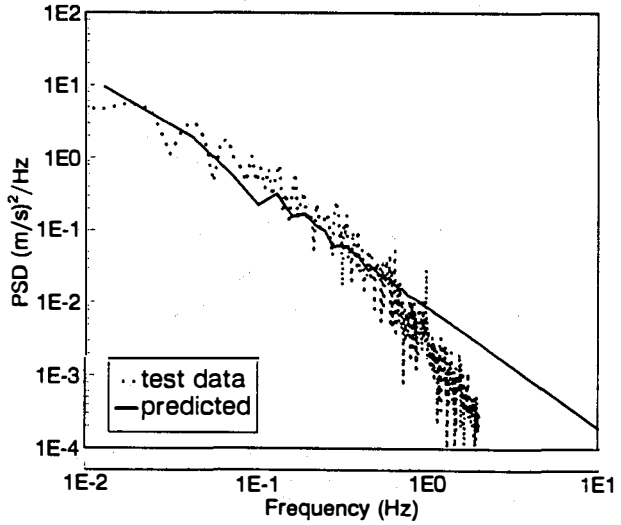

Figure 9. Spectra of Hubheight Anemometer (Case 2)

Code Inputs and Solution Methods

The STRAP code consists of two modules; module 1 is a preprocessor that reads blade and machine property data and prepares various matrices for use in the equations of motion. A feature of module 1 not previously reported is the ability to calculate the blade flapwise natural frequencies and modeshapes. This information is often helpful for checking input accuracy of the blade mass and stiffness data.

The second module solves blade equations of motion and calculates blade loads. Degrees of freedom include rotor rigid body teeter and elastic flapping motion of the blades. Inputs to the model include such deterministic effects as gravity, tower shadow, wind shear, yaw error and yaw rate. The code can also be run with a time series windspeed input to calculate stochastic blade responses caused by turbulence.

For this turbine, the rotor first and second symmetric flapwise bending modes were very close to 2P (2 per rev) and 8P (8 per rev), respectively. Besides the blade's distributed mass and stiffness inputs, inclusion of a 42-lb tip weight was crucial for correct calculations of rotor natural frequencies and loads. A power spectral density calculation of blade root bending moment shows significant response at 8P (see comparisons). This "tip brake" mass was modeled in STRAP by adding extra distributed mass over the last 2 ft of blade span. Other distributed blade properties are the blade's twist and chord distributions.

Besides distributed properties noted above, additional hub properties were input. Such effects as undersling and hub mass (mass not included as a part of the blade) were input, as seen in Figure 1. Neglect of these parameters causes an underprediction of the rotor's steady state response due to gravity, predominantly at a frequency of 1 Hz (1P). Exact values for this turbine's rotor and hub mass are not exactly known and may be the cause for some discrepancy in predicted 1P loads. This discrepancy will be described later.

Other inputs important to this turbine are correct wind shear and tower shadow data (this is a downwind machine). The power law shear coefficient was determined from the anemometer data. The tower shadow inputs are not well known. Both the wind shear and tower shadow cause blade elastic responses, which are amplified at the 2P and 8P frequencies, because of proximity of these frequencies to the rotor natural frequencies. Also of great importance is the inclusion of stochastic wind effects, which cause further excitation of the rotor, especially at these frequencies.

The first comparisons made in this paper are for deterministic responses only (steady state). For the 10-minute data sets, stationary operating conditions are assumed, and the deterministic and stochastic loads for the turbine test data are separated by "azimuth averaging."

The STRAP code is first run with only deterministic inputs of gravity, windshear and tower shadow. Case 1 had a small mean yaw error of 4°, while case 2 had a yaw error of 13°. Resulting teeter response and blade flap bending moment waveforms are calculated. The harmonic contents of these deterministic waveforms are also calculated by fitting a Fourier series with unknown coefficients in a "least squares" routine to both the test data and predicted waveforms.

Comparisons

After calculation of deterministic responses and loads, a transient solution subroutine is run in order to calculate stochastic responses. Data from a file containing rotationally sampled windspeeds, previously generated by VEERS model, is read by this subroutine at equal time steps.

The STRAP Code numerical integration procedure uses unequal time steps. For blade positions lying between those values from the

input file, linear interpolation is performed in order to obtain the necessary wind inputs to the blade.

All of the important blade and low-speed shaft loads such as blade flapwise and edgewise bending, shaft torque, etc., are calculated from both deterministic and turbulent inputs. In addition, rotor teeter response and blade elastic deflections are calculated.

Mean Loads

Table 4 shows mean shaft torque for each data case, predictions versus measured data. The code overpredicts torque, especially at the higher windspeed, due to errors in modeling lift and drag profiles at the higher angles of attack. For these runs, polynomial lift and drag profiles were modeled for angles of attack up to stall. Past stall, the VITTERNA poststall synthesization routine was used (7).

Table 5 shows mean flap-bending moment for the two cases at the root and 60% span locations. Unlike the torque comparisons, the flapwise bending moments agree better at the higher windspeed (case 1). The root bending moment for case 2 shows a 30% error; the exact cause of this discrepancy is not known. Usually the error in predicted mean bending moment is higher for the high windspeed case.

Table 4

PREDICTED VS MEASURED MEAN SHAFT TORQUE FOR THE TWO CASES

Case #	Predicted (ft-lb)	Measured (ft-lb)	% Error
1	35,400	25,900	37%
2	13.600	13.900	2%

Table 5

MEAN FLAP-BENDING MOMENT PREDICTED VERSUS MEASURED AT ROOT AND 60% BLADE STATIONS

Predicted (ft-lb)

Case #	Root	60% Span
1	22,400	3,350
2	5.480	1.020

Measured (ft-lb)

Case #	Root	60% Span
1	19,500	3,320
2	4.190	1.310

Deterministic Responses

A plot of predicted teeter waveform versus measured waveform is shown in Figures 10 to 11 for the two cases. In both cases the TEETER code predicts the total cyclic (peak-to-peak) teeter response reasonably, although the predicted waveforms are shifted in phase. The exact reasons for this discrepancy are unknown.

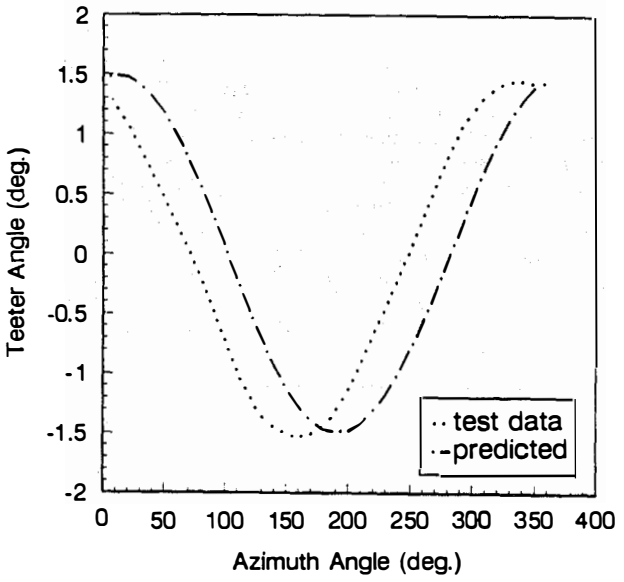

Figure 10. Plot of Teeter Response (Case 1)

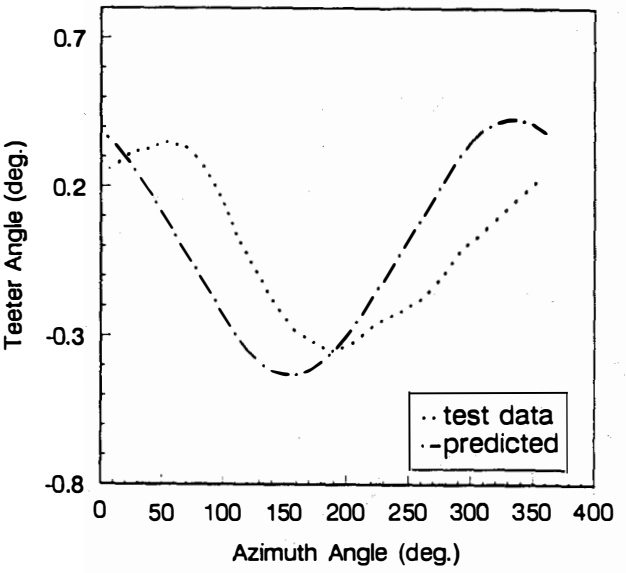

Figure 11. Plot of Teeter Response (Case 2)

Important parameters for this machine to include in the analytical model were: (1) hub geometry such as the rotor undersling and hub mass, (2) blade tip mass effects, and (3) windshear and tower shadow.

Figures 12 through 15 show the harmonic content of the deterministic root and 60% span flap-bending moments for the two cases. In case 1, two predictions are shown: the first prediction is with a tower shadow having a velocity deficit of 20% of the mean windspeed over a pie-shaped sector centered at the tower with half-width of 10°. The second prediction is with a 30% deficit over a sector with half-width of 15°. The change in 2P and 8P content is clear.

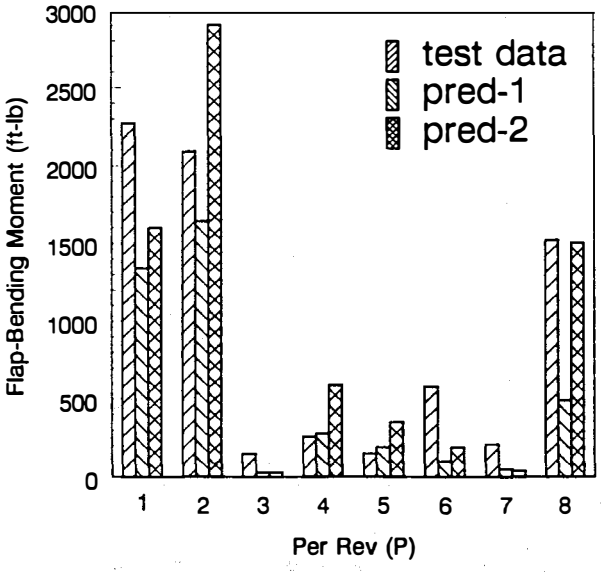

Figure 12. Plot of Root Flap Moment Harmonics (Case 1)

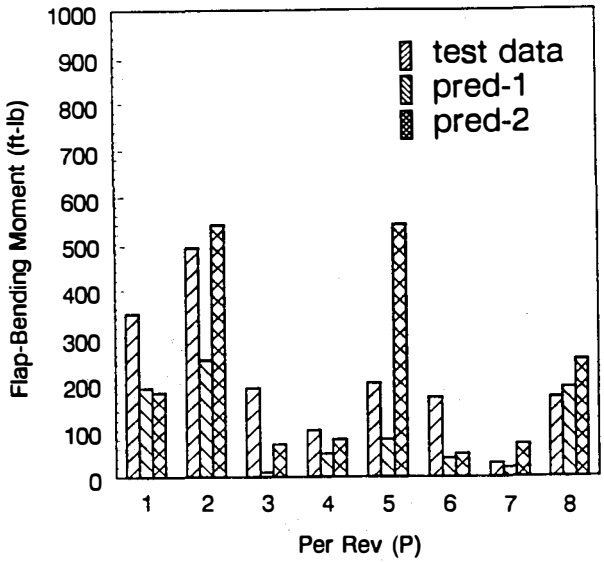

Figure 13. Plot of 60% Span Flap Moment Harmonics (Case 1)

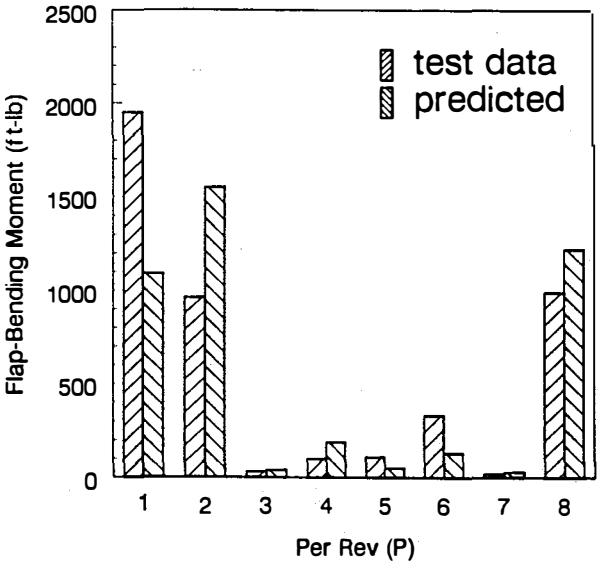

Figure 14. Plot of Root Flap Moment Harmonics (Case 2)

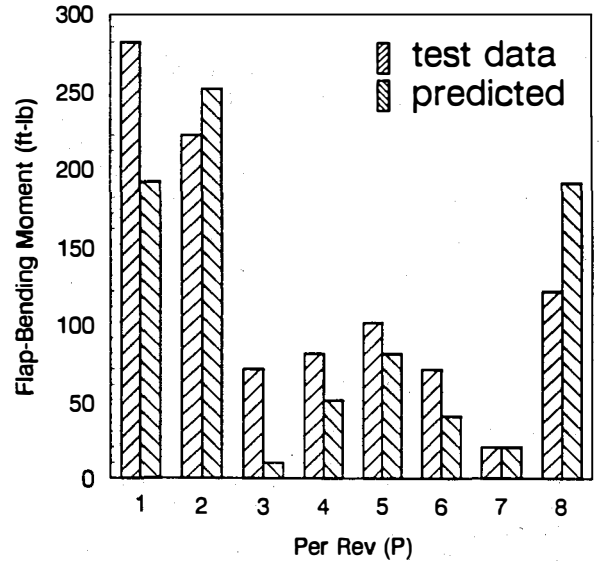

Figure 15. Plot of 60% Span Flap Moment Harmonics (Case 2)

The dominant frequencies of interest for this rotor are at 1P, 2P, and 8P (1 Hz, 2 Hz, and 8 Hz). The 1P harmonic content is due mainly to rotor response to gravity. The magnitude of this harmonic is relatively constant for the two windspeed cases. The 2P harmonic is due mainly to excitation of the rotor symmetric flap mode by aerodynamic inputs, such as windshear and tower shadow. It is underpredicted in case 1 for the first tower shadow case and overpredicted for the second value.

The 8P harmonic is caused by excitation of the rotor's second symmetric flap mode by windshear and tower shadow. The rotor asymmetric flap mode, which has a frequency close to 5P (5 Hz) is not highly excited in this rotor, although some response is noted at this frequency for the 60% span station. The code seems to overpredict response at this frequency for the higher tower shadow deficit. Both of these harmonics are highly influenced by the tower shadow velocity deficit, as seen in figures 12 and 13.

For both cases 1 and 2, the 1P harmonic is underpredicted by about 40%. This discrepancy is thought to be due to underestimation of the total rotor and hub weight or lack of knowledge of the exact rotor center of gravity location. This harmonic is dominated by gravity response. More detailed knowledge of these weights and offsets would allow improved prediction of this harmonic.

For case 2, the 2P and 8P harmonics are overpredicted. This discrepancy is thought to be due to inaccurate information regarding tower shadow effects. Accurate estimates of the power law windshear coefficient were obtained by analyzing the anemometer data at three heights. The tower shadow was modeled as a pie-shaped sector, with a half-width of 10° centered about the tower centerline with a velocity deficit of 20%. When harmonics are compared for case 2, with the shadow velocity deficit reduced to 10%, the predicted 2P and 8P harmonics drop significantly. Again, the 1P harmonic is underpredicted, as in case 1.

Another important parameter in this rotor analysis is the 42-lb tip mass. This tip mass causes the blade's second symmetric flap mode to be very close to 8P. Because of the proximity of this mode to an even harmonic of the rotor speed, it gets highly excited by wind shear and tower shadow. Figure 16 shows a reduction in higher harmonic (8P) content of the root flap moment waveform, as the tip mass is reduced from 42 lb to 0 lb.

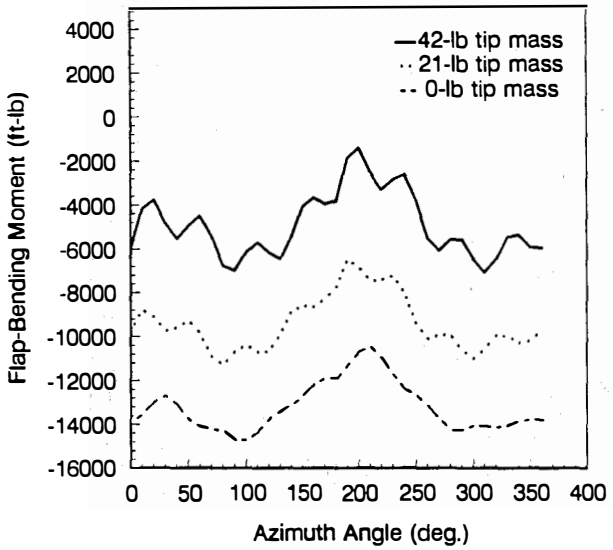

Figure 16. Effects of Tip Mass on Predicted Flap Moment Waveforms (Case 2)

As the tip mass is reduced, the blade's second symmetric flap frequency moves away from the 8P harmonic. Excitation at this frequency is reduced. Prediction of these effects requires that the rotor code has a sufficient number of degrees of freedom; in this case, the model must include the second symmetric flap mode. Analyses using just two modes, such as rigid body teeter and first symmetric flap, would underestimate response at higher frequencies.

Another effect of tip mass removal is the change in mean flap moments, also seen in Figure 16. This is caused by the change in centrifugal loads at the blade tip.

Stochastic Responses

The VEERS turbulence model (5) was run for these two data cases to produce a time series of turbulent windspeed data to be input to STRAP. For case 1, the VEERS code was run twice: once with a value of CODEC = 7 (PRED-1) and the other time with a value of CODEC = 15 (PRED-2). This was done to show the effects of coherency parameter on predicted teeter and flapwise moment predictions.

Figures 17 to 18 show predicted teeter response power spectral densities compared to test data, for cases 1 and 2. For case 1, better results are obtained for prediction-1, in which the value of CODEC = 7 was used. Overall, the test data show a broad band response in the vicinity of the 1P frequency. The predictions underestimated this response. One possible explanation for this discrepancy could be due to neglect of wind excitation in the other directions. In this analysis, only longitudinal (along wind) turbulence components have been input to STRAP. Components in the lateral and vertical directions could influence this turbine's response. The STRAP code can be easily modified to include calculations for these other inputs, and further investigations will be made. The VEERS model, however, must also be modified to output turbulent wind excitations in the other directions.

In case 2, the value of CODEC was set at 15. The dominant response in teetering for this case is also at, or close to, a frequency of 1P. The agreement between test data and predictions is much better for this case than case 1. Also, the magnitude of the response for case 1 is about 10 times that of case 2, probably due to the higher turbulence intensity and shear value for this case.

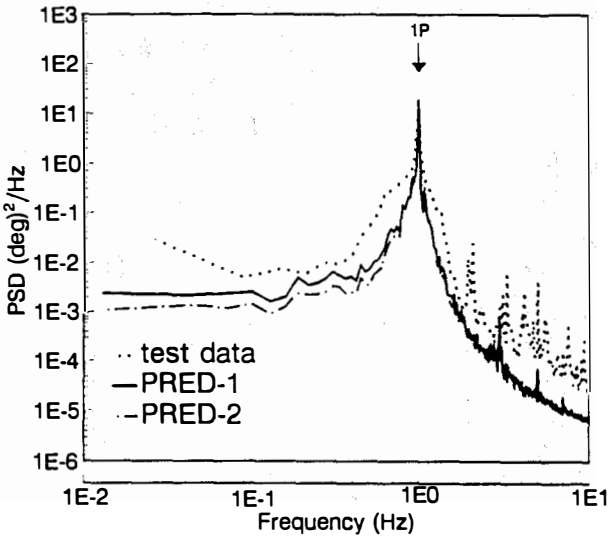

Figure 17. Plot of Teeter Power Spectral Density (Case 1)

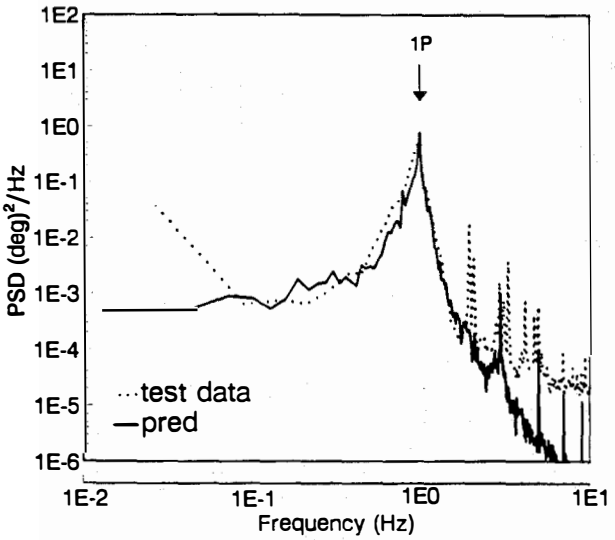

Figure 18. Plot of Teeter Power Spectral Density (Case 2)

Figures 19 and 20 show power spectral densities of root flap-bending moment for the two cases. The dominant response of the rotor is at the frequencies 1 Hz, 2 Hz, and 8 Hz, although some response is noted at 6 Hz (6P).

The 1 hertz (1P) response is again due to response of the rotor to gravity. The magnitude of this frequency response does not change much for the two data cases.

The 2 hertz (2P) frequency response is due mainly to excitation of the first symmetric flap mode by wind turbulence, wind shear and tower shadow. The 8 hertz (8P) response is also due to excitation by these effects. Response at these frequencies is seen to go up for the higher windspeed case.

Predictions for case 1 are shown for two conditions. Prediction-1 is for a value of CODEC = 7, and prediction-2 is for a case with CODEC = 15. The change in coherence seems to effect the low frequency portion of the spectrum (below 1 hz) with the value of CODEC = 7 giving better results. Also to be noted in case 1 is the large underprediction in the high frequency range between 6 and 8 hertz. This underprediction is not noted for the lower windspeed case

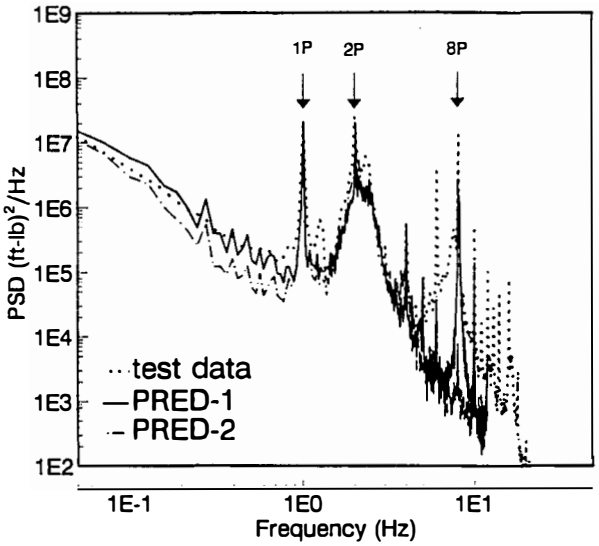

Figure 19. Plot of Root Flap Moment PSD (Case 1)

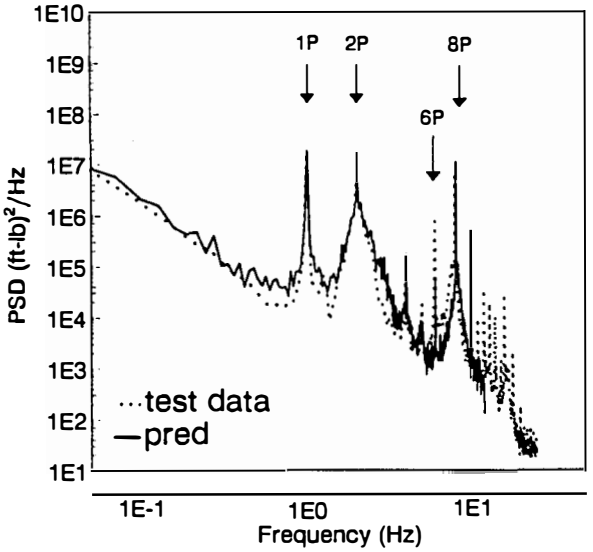

Figure 20. Plot of Root Flap Moment PSD (Case 2)

2. It is not known at this time the cause of this underprediction although it is known that the rotor blade is highly stalled at this windspeed. Not modeled in STRAP is the blade edgewise degree of freedom. It is also known that the blade first edgewise frequency is at approximately 6 hertz.

Conclusions

The STRAP [NREL (formerly SERI) Teetering Rotor Analysis Program] has been reviewed and shown to be applicable for estimation of both deterministic and stochastic rotor response. The code accounts for such hub properties as rotor teeter motion, delta-3 hinge geometry, undersling and ability to include a concentrated hub mass. Blade elastic flap motion is also included. The effects of turbulent wind inputs are also included.

Code response and load predictions were compared to measurements taken from a two-bladed, downwind, stall controlled test turbine with a teetering hub geometry.

The 1P harmonic is strongly influenced by gravity response, while the 2P and 8P responses are strongly influenced by shear and shadow. The 1P teeter response is also strongly influenced by shear and wind turbulence.

An important parameter for this rotor analysis was the 42-lb tip mass. Both cyclic response at the 8P harmonic and mean loads were shown to be strongly influenced by this weight.

Stochastic load comparisons were shown for both cases. The VEERS turbulence model was used to prepare a file of turbulent wind inputs for STRAP. Power spectral densities of rotor teeter and flap-bending moments showed reasonable agreement for both cases. One unknown parameter for these cases was the coherence decrement, not determined from the anemometer data. This parameter has an effect on predicted teeter and flap load prediction, especially in the low frequency range. For future load comparisons, more accurate estimates of this parameter should be used.

A major goal of future NREL research (through subcontracted efforts with the University of Utah) is to develop more sophisticated aerodynamic models for inclusion in structural dynamic models. It is clear that even with accurate modeling of the static lift and drag profiles for this airfoil, STRAP aerodynamic models need further refinement for calculating cyclic response at higher windspeeds. Unsteady aerodynamic models may be needed to accurately predict dynamic loading. This is particularly true for stall controlled rotors as has been shown by experimental results from the NREL Combined Experiment tests in (9) and (10). These tests have shown that delayed stall occurs for smooth and rough airfoils. Even with accurate modeling of lift and drag for the higher windspeed, cyclic response was underestimated for this rotor, especially at higher frequencies.

Another area of interest is development of more sophisticated structural models with more degrees of freedom. At the present time, no additional degrees of freedom are planned for STRAP. Systems code development work is planned through subcontracted efforts (Oregon State University) as well as through in-house efforts with a commercial software multi-body dynamics code, the Automated Dynamic Analysis of Mechanical Systems (ADAMS) (11).

References

1. Wright, A. D., and Thresher, R. W., Prediction of Stochastic Blade Responses Using Measured Wind-Speed Data as Input to FLAP, SERI/TP-217-3394, Solar Energy Research Institute, Golden, Colorado, November 1988.

2. Thresher, R. W., Holley, W. E., and Wright, A. D., Prediction of Stochastic Blade Responses Using a Filtered Noise Turbulence Model in the FLAP Code, SERI/TP-217-3413, Solar Energy Research Institute, Golden. Colorado, November 1988. Also presented at the 8th ASME Wind Energy Symposium, Houston, Texas, January 22-26, 1989.

3. Wright, A. D., et al., Prediction of Stochastic Blade Loads for Three-Bladed, Rigid Hub Rotors, SERI/TP-257-3589, Solar Energy Research Institute, Golden, Colorado, November 1989.

4. Wilson, R. E., Walker, S. N., Hartin, J. R., and Weber, T. L., Load Response of Horizontal-Axis Wind Turbine to Turbulence, SERI/TP-257-3891, Solar Energy Research Institute, Golden, Colorado, September 1990.

5. Veers, P. S., Three-Dimensional Wind Simulation, SAND 88-0152, Sandia National Laboratories, Albuquerque, New Mexico, March 1988.

6. Wright, A. D., Buhl, M. L., and Thresher, R. W., FLAP Code Development and Validation, SERI/TR-217-3125, Solar Energy Research Institute, Golden, Colorado, 1988.

7. Viterna, L. A. and Corrigan, R. D., "Fixed Pitch Rotor Performance of Large HAWTs," paper presented at the DOE/NASA workshop on large HAWTs, Cleveland, Ohio, July 28-30, 1981.

8. Weber, T. L., Inclusion of Nonlinear Aerodynamics in the FLAP Code, SERI/TP-257-3558, Solar Energy Research Institute, Golden, Colorado, November 1989.

9. Butterfield, C. P., Aerodynamic Pressure and Flow Visualization Measurements from a Rotating Wind Turbine Blade, SERI/TP-217-3433, Solar Energy Research Institute, Golden, Colorado, November 1988.

10. Musial, W. D., Butterfield, C. P., and Jenks, M. D., A Comparison of Two- and Three-Dimensional S809 Airfoil Properties for Rough and Smooth HAWT Rotor Operation, SERI TP-257-3603, Solar Energy Research Institute, Golden, Colorado, February 1990.

11. Elliott, A. S., and McConville, J. B., "Analyzing Rotor Dynamics with a General Purpose Code," Mechanical Engineering, December 1990.

12. Winkelaar, D., Fast Three-Dimensional Wind Simulation and the Prediction of Stochastic Blade Loads, presented at the Tenth ASME Wind Energy Symposium, Houston, Texas, January 20-23, 1991.